Imaging and etiologic spectrum of cavernous sinus syndrome: a retrospective observational study of 26 patients

Wiame Bougrine[1,2*], Brahim El Mahjoub [1,2], Hajar Ouazzani Chahdi[2], Ismail Chaouche[1], Amal Akammar[2], Nizar El Bouardi[1], Meriem Haloua[2], Badreeddine Alami[1], Mly Youssef Alaoui Lamrani[1], Mustapha Maaroufi[1], Meryem Boubbou[2]

European Journal of Medical Case Reports
Volume 10(10):336–346
DOI: 10.24911/ejmcr.9-2809

ABSTRACT

Background: Cavernous sinus syndrome (CSS) is an uncommon yet potentially life-threatening condition resulting from neoplastic, vascular, or inflammatory lesions with overlapping clinical characteristics. Early and precise imaging is crucial for guiding prompt management and preventing severe complications.

Aims and Objectives: The study aims to outline the etiological distribution and imaging characteristics of CSS in a North African tertiary care cohort and assess the role of multimodal imaging in determining the underlying diagnosis.

Settings: Radiology Department, University Hospital Hassan II, Fez, Morocco (January 2021–December 2024).

Methods: This retrospective observational study involved 26 consecutive patients. All patients underwent contrast-enhanced computed tomography, and magnetic resonance imaging was performed in 13 patients (50%) with MR angiography/venography as required. Imaging findings underwent independent review by two senior radiologists, with any disagreements resolved through consensus. Diagnoses were confirmed using histopathology, angiography, hormonal assays, microbiological workup, or clinical and therapeutic responses, as appropriate.

Results: The mean age of the patients was 49 ± 18 years, with 14 men and 12 women. Neoplastic causes were predominant (*n* = 16; 62%), including meningioma (*n* = 5), pituitary macroadenoma (*n* = 4), undifferentiated carcinoma of nasopharyngeal type (*n* = 2), lymphoma (*n* = 2), cavernous hemangioma (*n* = 1), chordoma (*n* = 1), and chondrosarcoma (*n* = 1). Vascular causes constituted 31% of the cases, including cavernous sinus thrombosis (*n* = 4), carotid-cavernous fistulas (*n* = 2), and aneurysms (*n* = 2). Inflammatory causes accounted for 8% of the cases, including Tolosa–Hunt syndrome and orbital pseudotumor. Computed tomography provided a working diagnosis in all cases, while magnetic resonance imaging offered superior soft-tissue characterization and vascular delineation when available.

Conclusion: Multimodal imaging contributed to etiological characterization and management planning in this cohort. Neoplastic and vascular causes were predominant in this North African cohort, with an etiologic distribution differing from those reported in Western and South Asian series. Systematic imaging evaluation is crucial to prevent diagnostic delays and guide appropriate management of potentially reversible or life-threatening conditions.

Keywords: Cavernous sinus syndrome, painful ophthalmoplegia, multimodal imaging, cavernous sinus thrombosis, Tolosa–Hunt Syndrome, carotid-cavernous fistula.

Type of Article: Original article **Specialty:** Radiology

Correspondence to: Wiame Bougrine
*Department of Adult Radiology, University Hospital CHU Hassan II, Faculty of Medicine and Pharmacy, Sidi Mohamed Ben Abdellah University, Fez, Morocco.
Email: wiame.bougrine@gmail.com
Full list of author information is available at the end of the article.

Received: 10 April 2026
Revised (1): 05 June 2026
Revised (2): 12 August 2026
Revised (3): 06 August 2026
Accepted: 24 August 2026

Introduction

The cavernous sinus is a complex dural venous space situated on each side of the sella turcica, crossed by the internal carotid artery and several cranial nerves, such as the oculomotor (III), trochlear (IV), trigeminal (V1 and V2), and abducens (VI) nerves. Lesions that affect this area result in cavernous sinus syndrome (CSS), characterized by painful ophthalmoplegia and cranial nerve dysfunction.

CSS encompasses neoplastic, vascular, inflammatory, and infectious causes [1]. Early diagnosis is crucial due to the risk of rapid progression and complications such as vision loss, stroke, or intracranial extension.

Computed tomography (CT) offers a quick evaluation of bony structures and acute issues, while magnetic resonance imaging (MRI) with contrast enhancement and angiographic sequences allows for thorough characterization of soft tissues and evaluation of vascular involvement and perineural spread [2,3].

Its etiological distribution varies across geographic regions, reflecting variations in epidemiology and

healthcare access [1,4]. However, there are limited data on North African populations.

This study outlines the etiologic distribution and imaging characteristics of CSS in a retrospective observational cohort from a North African tertiary center, highlighting the role of multimodal imaging in establishing the underlying diagnosis.

Materials and Methods

Study design and population

This retrospective observational study was conducted at the Radiology Department of University Hospital Hassan II, Fez, Morocco. The study involved reviewing consecutive patients referred for suspected CSS between January 2021 and December 2024. Ethical approval was obtained from the Comité d'Éthique Hospitalo-Universitaire de Fès (approval number: 02/2025) prior to data extraction, analysis, and manuscript preparation. Although the clinical records reviewed span the period from January 2021 to December 2024, all data were extracted retrospectively from existing medical records following ethics approval in 2025. No prospective data collection or patient contact was performed. The study was conducted in accordance with the ethical principles of the Declaration of Helsinki.

Written informed consent was obtained from all 26 patients, covering participation in the study and publication of clinical data and accompanying images. For the pediatric patient, consent was obtained from the parents. For the deceased patient, consent was obtained from the next of kin. For patients lost to follow-up, consent was obtained at their last available clinical visit.

A total of 39 patients were initially screened. Of these, 13 were excluded due to incomplete imaging studies or clinical conditions unrelated to cavernous sinus pathology. The remaining 26 consecutive patients who met all inclusion criteria were enrolled (Figure 1).

The inclusion criteria were as follows: (1) clinical presentation consistent with CSS, defined as at least one of the following - orbital or periorbital pain, diplopia, or visual impairment - associated with paresis of at least one cranial nerve traversing the cavernous sinus (CN II, III, IV, V1, V2, or VI) and (2) availability of diagnostic-quality CT and/or MRI. The exclusion criteria included incomplete imaging studies or clinical conditions unrelated to cavernous sinus pathology.

Imaging protocol

All patients underwent multidetector CT with non-contrast and contrast-enhanced imaging. MRI was performed in 13 patients (50%) using a 1.5 T system, which included axial and coronal T1-, T2-, FLAIR-, and diffusion-weighted sequences, along with fat-suppressed post-gadolinium T1-weighted images. MR angiography () and/or MR venography (MRV) were conducted if vascular pathology was suspected. In patients who did not undergo MRI, the diagnosis relied on CT combined with clinical assessment, angiographic data, or histopathological confirmation as appropriate.

Image analysis

Two senior neuroradiologists, who were blinded to each other's interpretations, independently reviewed all studies. Discrepancies were resolved by consensus, with clinician

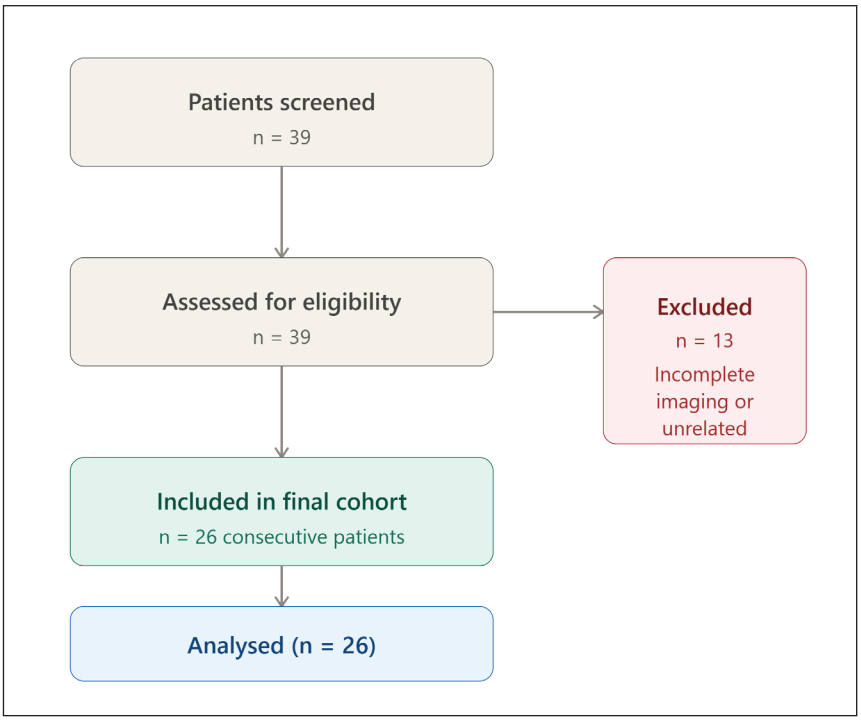

Figure 1. *Flowchart illustrating the patient selection process.*

input when necessary. The lesion's location, morphology, signal characteristics, and enhancement patterns were systematically documented.

Data collection and analysis

Clinical data were obtained from medical records. Final diagnoses were established through imaging, histopathology, hormonal assay, microbiological workup, angiographic confirmation, or therapeutic response, and classified as neoplastic, vascular, or inflammatory.

Clinical outcomes were assessed at the last available follow-up visit, with a follow-up period ranging from 2 to 36 months, and categorized as complete resolution, good recovery, partial recovery, slight improvement, stable, or no recovery, based on cranial nerve function, and symptom status. Patients with no available post-treatment assessment were classified as lost to follow-up.

Descriptive statistics were utilized, with continuous variables presented as mean ± standard deviation and categorical variables as frequencies and percentages.

Results

Demographics and clinical presentation

The cohort consisted of 26 patients (14 men, 12 women; male-to-female ratio 1.17:1), with a mean age of 49 ± 18 years (range, 6–83 years).

The predominant symptoms included orbital pain (21 patients, 81%), diplopia (24 patients, 92%), ptosis (15 patients, 58%), headache (14 patients, 54%), and visual impairment (4 patients, 15%). Complete ophthalmoplegia, defined as simultaneous involvement of CN III, IV, and VI, was observed in 4 patients (15%).

Cranial nerve involvement reflected the typical anatomical arrangement of the cavernous sinus. CN VI was the most commonly affected nerve (23 patients, 88%), followed by CN III (15 patients, 58%) and CN IV (12 patients, 46%). CN V1 was affected in 19 patients (73%), CN V2 in 4 patients (15%), and CN II in 4 patients (15%), the latter exclusively in advanced or compressive pathology.

Symptom onset was acute (less than one week) in 8 patients (31%), primarily due to vascular causes, while neoplastic and inflammatory conditions exhibited a more gradual progression.

Imaging findings

CT was performed in all 26 patients, providing rapid evaluation of bony structures, mass effects, and vascular complications. MRI, performed in 13 patients (50%), provided superior soft-tissue characterization, assessment of perineural spread, and vascular delineation. MRI was unavailable for the remaining 13 patients due to resource constraints; in these cases, diagnosis relied on CT combined with clinical, angiographic, or histopathological data.

Neoplastic causes accounted for 16 cases (62%), vascular causes for 8 (31%), and inflammatory causes for 2 (8%). Diagnostic confirmation was achieved by

Table 1. *Clinical and imaging characteristics, diagnostic confirmation, and treatment outcomes of 26 patients with cavernous sinus syndrome.*

#	Sex	Age	Presenting symptoms	Cranial nerves involved	Imaging	Final diagnosis	Confirmation method	Treatment / outcome
1	M	6	Orbital pain, diplopia	IV, VI, V1	CT	**Lymphoma**	Biopsy of lymph nodes + histopathology + immunohistochemistry	Chemotherapy; complete resolution
2	F	17	Pain, diplopia, ptosis	III, IV, VI, V1	CT + MRI	**Inflammatory pseudotumor**	Imaging + exclusion of infection/malignancy + steroid response	Corticosteroids; good response, follow-up for recurrence
3	F	28	Pain, diplopia, ptosis, headache	III, VI, V1	CT + MRI	**Carotid-cavernous fistula**	Digital subtraction angiography (DSA)	Endovascular embolization; good recovery of orbital signs
4	F	32	Pain, diplopia, ptosis, headache	III, IV, VI, V1	CT + MRI	**Tolosa-Hunt syndrome**	Imaging + exclusion of mimics + corticosteroid response	Corticosteroids; complete resolution
5	M	35	Pain, diplopia, ptosis, headache, complete ophthalmoplegia	III, IV, VI, V1, V2	CT	**Cavernous sinus thrombosis complicating an orbital cellulitis**	CT filling defect; clinical + microbiological workup	Anticoagulation + antibiotics; good recovery
6	F	38	Diplopia, headache, visual impairment	VI, II	CT	**Pituitary macroadenoma**	Imaging (sellar origin, ICA encasement) + histopathology after surgery	Transsphenoidal surgery; only partial recovery of the symptoms
7	M	40	Pain, diplopia, ptosis, headache	III, IV, VI, V1, V2	CT	**Undifferentiated carcinoma of nasopharyngeal type**	Nasopharyngeal biopsy + histopathology	Chemoradiotherapy; partial response

#	Sex	Age	Presenting symptoms	Cranial nerves involved	Imaging	Final diagnosis	Confirmation method	Treatment / outcome
8	F	42	Pain, diplopia, ptosis, headache	III, IV, VI, V1, V2	CT	**Meningioma**	Imaging features (dural tail, hyperostosis)	Subtotal surgical resection + radiotherapy; stable CN function
9	M	44	Pain, diplopia, ptosis, headache	III, IV, VI, V1	CT	**Cavernous sinus thrombosis complicating a sphenoidal sinusitis**	CT filling defect; clinical + microbiological workup	Anticoagulation + antibiotics; partial recovery
10	F	45	Diplopia, headache	VI	CT + MRI	**Pituitary macroadenoma**	Imaging + histopathology after surgery	Transsphenoidal surgery; improved
11	M	46	Pain, diplopia, ptosis, headache	III, VI, V1	CT + MRI	**Carotid-cavernous fistula**	CT/MRA initial detection; DSA confirmation	Endovascular embolization; good recovery
12	F	47	Pain, diplopia, ptosis	III, IV, VI, V1	CT + MRI	**Meningioma**	Imaging features	Radiotherapy; slight improvement of CN function
13	M	48	Pain, diplopia, ptosis, headache	III, IV, VI, V1, V2	CT	**Undifferentiated carcinoma of nasopharyngeal type**	Nasopharyngeal biopsy + histopathology	Chemoradiotherapy; partial response
14	F	49	Pain, diplopia, ptosis	III, IV, VI, V1	CT	**Meningioma**	Imaging features	Radiotherapy; stable CN function
15	M	50	Pain, diplopia, ptosis, headache	III	CT + MRI	**Aneurysm (PCom)**	CT/MR angiography + DSA confirmation	Endovascular coiling; CN III recovery after decompression
16	F	51	Pain, diplopia, ptosis, headache	III, IV, VI, V1	CT	**Cavernous sinus thrombosis complicating a sphenoidal sinusitis**	CT filling defect; clinical workup	Anticoagulation + antibiotics; partial recovery
17	M	52	Headache, visual impairment	II	CT + MRI	**Pituitary macroadenoma**	Imaging + hormonal assay	Transsphenoidal surgery; partial visual recovery
18	F	58	Pain, diplopia	V1, VI	CT + MRI	**Meningioma**	Imaging features	Patient lost to follow-up
19	M	60	Pain, diplopia, ptosis	III, VI	CT + MRI	**Aneurysm (ICA)**	CT/MR angiography + DSA confirmation	Surgical clipping; partial recovery
20	F	63	Pain, diplopia, visual impairment	II, V1, VI	CT	**Meningioma**	Imaging features + histopathology after surgery	Subtotal surgical resection + radiotherapy; no CN function recovery
21	M	65	Pain, diplopia	VI, V1	CT + MRI	**Chordoma**	Imaging features	Patient lost to follow-up
22	M	67	Pain, diplopia	VI, V1	CT	**Chondrosarcoma**	Imaging features	Deceased
23	F	67	Headache, visual impairment	II	CT	**Pituitary macroadenoma**	Imaging + hormonal assay	Transsphenoidal surgery; no visual recovery
24	M	70	Progressive diplopia	VI	CT + MRI	**Cavernous hemangioma**	Imaging features (T2 hyperintensity, progressive enhancement)	Observation; stable, good prognosis
25	M	71	Pain, diplopia, ptosis, headache	III, IV, VI, V1	CT + MRI	**Cavernous sinus thrombosis complicating orbital cellulitis**	CT/MRV filling defect; clinical + microbiological workup	Anticoagulation + antibiotics; partial recovery
26	M	83	Pain, diplopia	VI, V1	CT	**Lymphoma**	Biopsy + histopathology + immunohistochemistry	Chemotherapy; good recovery

histopathology in 7 patients, digital subtraction angiography (DSA) in 4, imaging combined with hormonal assay in 2, and imaging features alone or combined with clinical and therapeutic response in the remaining 13 cases (Table 1).

1. Neoplastic etiologies (*n* = 16, 62%)

Neoplastic lesions were the most frequent cause of CSS in this cohort. The most prevalent tumors included meningiomas (*n* = 5) and pituitary macroadenomas (*n* = 4), followed by undifferentiated carcinoma of nasopharyngeal type (UCNT, *n* = 2), lymphoma (*n* = 2), cavernous hemangioma (*n* = 1), chordoma (*n* = 1), and chondrosarcoma (*n* = 1). Lesions typically appeared as expansile parasellar or skull base masses with moderate to intense contrast enhancement.

Meningiomas were diagnosed based on characteristic imaging features, including an extra-axial enhancing mass, dural tail, and bone remodeling, with histopathological confirmation in one surgically resected case. Outcomes varied: one patient showed no postoperative cranial nerve recovery, one was lost to follow-up, and the remainder demonstrated stable or slight improvement (Figure 2).

Pituitary macroadenomas showed sellar enlargement with lateral cavernous sinus extension, occasionally surrounding the intracavernous internal carotid artery without luminal narrowing. Diagnosis was based on imaging and hormonal assay in two cases and histopathology following transsphenoidal surgery in the other two. All four patients underwent transsphenoidal surgery with variable outcomes.

UCNT presented as infiltrative nasopharyngeal masses with skull base invasion, confirmed by biopsy and histopathology in both cases. Both patients received chemoradiotherapy with partial response.

Lymphomas appeared as homogeneously enhancing infiltrative lesions, confirmed by lymph node biopsy and

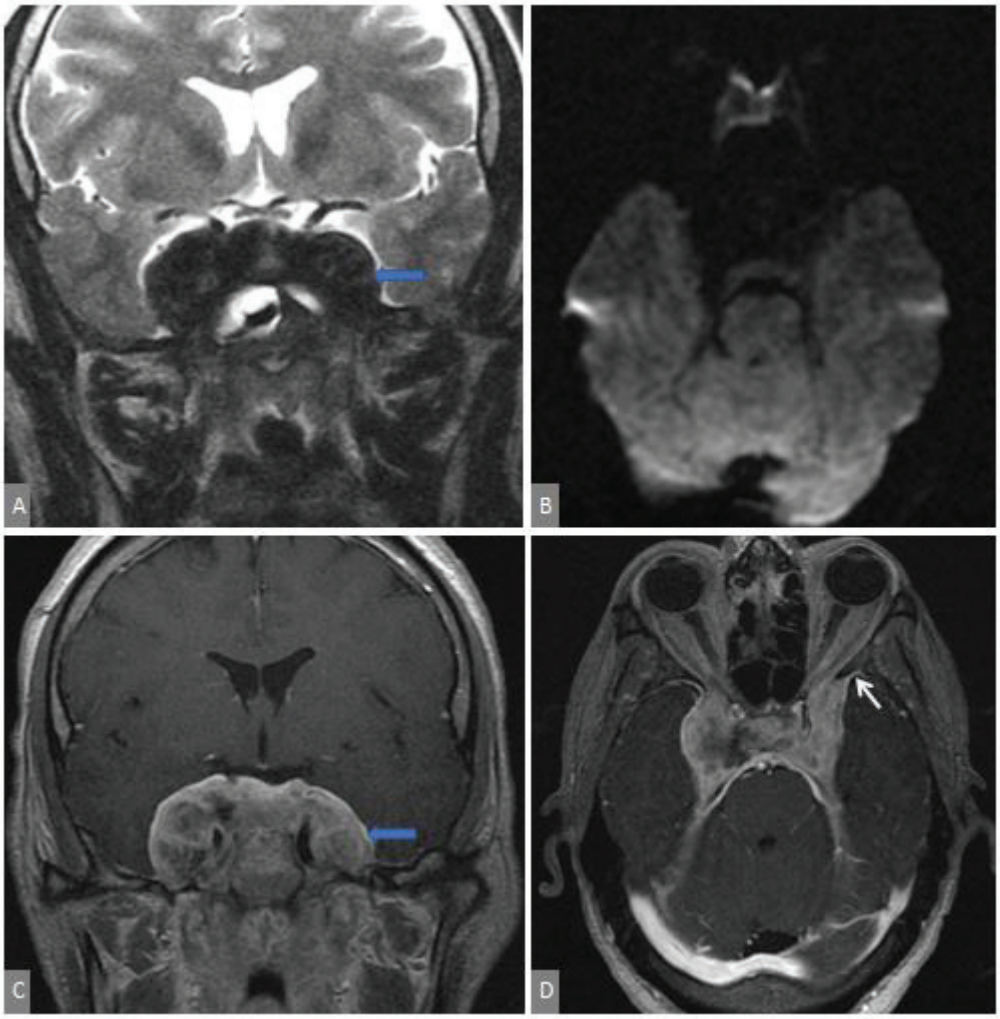

Figure 2. *A 58-year-old woman presenting with a 3-week history of bilateral painful ophthalmoplegia. Coronal T2-weighted MRI (1.5 T) (a) demonstrates a well-defined extra-axial lesion with bilateral cavernous sinus involvement, appearing hypointense relative to brain parenchyma, consistent with its fibrous composition. Axial diffusion-weighted imaging (b) shows no diffusion restriction. Coronal (c) and axial (d) post-gadolinium T1-weighted images demonstrate heterogeneous enhancement with a dural tail sign (white arrow), consistent with cavernous sinus meningioma. All images are fully anonymized and reproduced with written patient consent.*

immunohistochemistry. One patient, a 6-year-old child, achieved complete resolution, while the other showed good recovery after chemotherapy.

Cavernous hemangioma presented with progressive painless diplopia and subtle CN VI involvement. MRI demonstrated a well-defined T2-hyperintense lesion with progressive enhancement; the patient was managed conservatively with stable follow-up.

Both chordoma and chondrosarcoma were aggressive skull base lesions identified through imaging features alone. Tissue sampling was not performed in these two cases owing to the clinical condition of the patients; diagnoses were based on characteristic imaging features and discussed in a multidisciplinary setting. The patient with chordoma was lost to follow-up, while the patient with chondrosarcoma deceased (Figure 3).

2. Vascular etiologies (n = 8, 31%)

Vascular causes comprised cavernous sinus thrombosis (CST, n = 4), carotid-cavernous fistulas (CCF, n = 2), and intracranial aneurysms (n = 2; one involving the internal carotid artery and one the posterior communicating artery).

CST presented as intraluminal CT filling defects, accompanied by absence of MRI flow voids and engorgement of the superior ophthalmic vein. All four cases were of septic origin: two complicated orbital cellulitis and two sphenoidal sinusitis. MRV was performed in one patient. All patients received anticoagulation and antibiotics; one

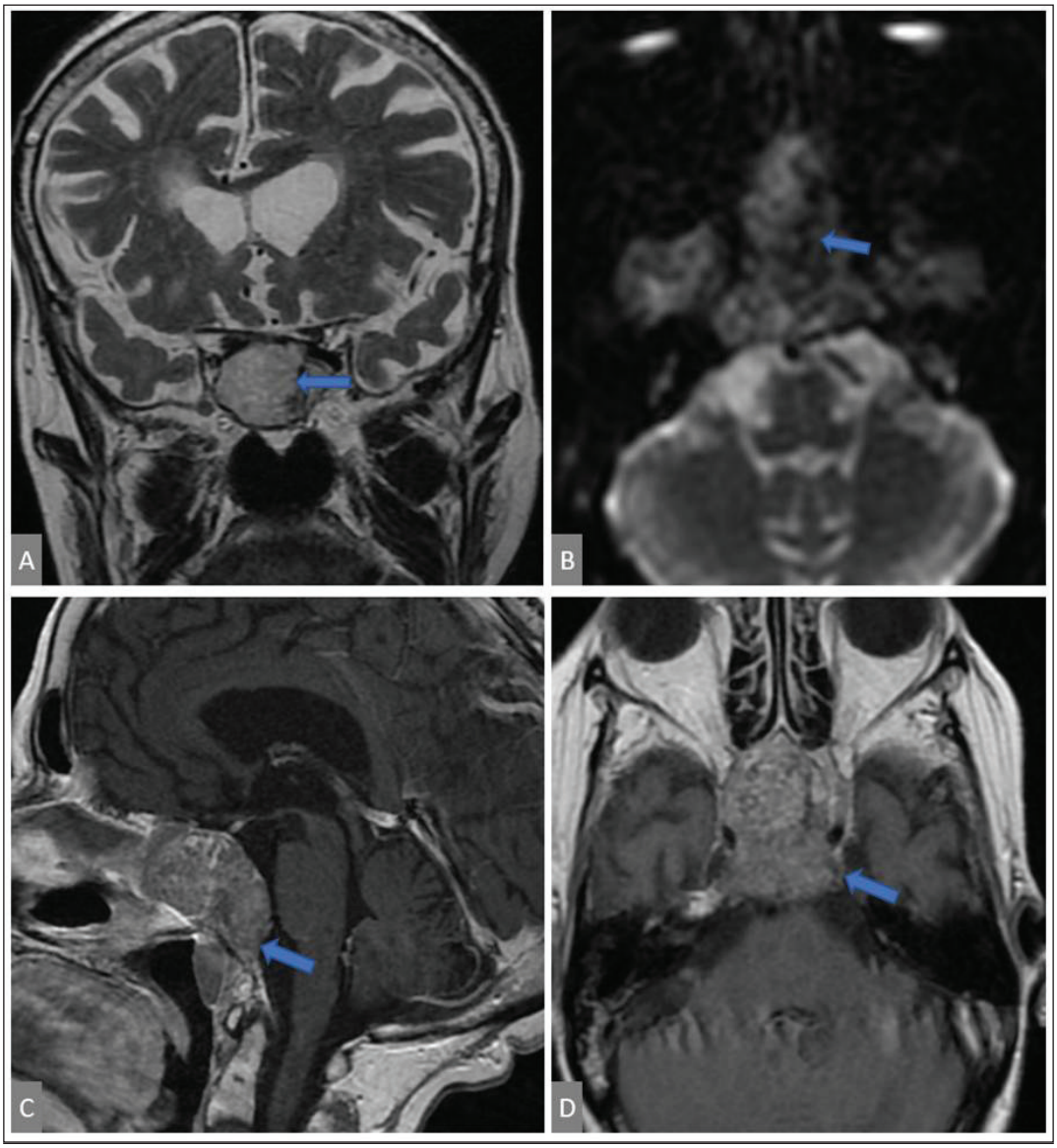

Figure 3. *A 65-year-old man presenting with a 2-week history of progressive bilateral ophthalmoplegia, visual disturbances, and headache. Coronal T2-weighted MRI (1.5 T) (a) demonstrates a lobulated clival and sphenoid body mass with heterogeneous signal, including areas of T2 hyperintensity reflecting the myxoid matrix of chordoma. Axial diffusion-weighted imaging (b) shows no significant diffusion restriction. Sagittal (c) and axial (d) post-gadolinium T1-weighted images reveal moderate heterogeneous enhancement with aggressive local extension involving both cavernous sinuses, the pituitary gland, the sphenoid sinus, and the right orbital apex, consistent with clival chordoma. All images are fully anonymized and reproduced with written patient consent.*

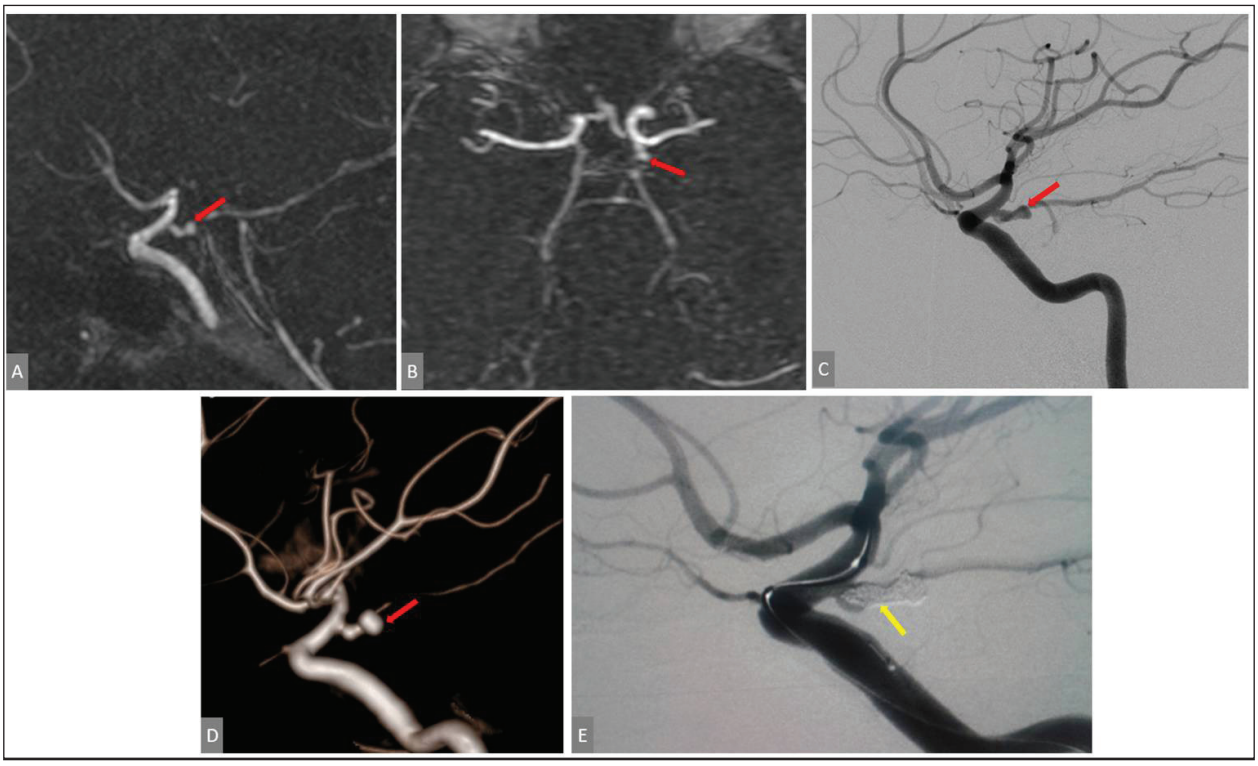

Figure 4. *A 50-year-old man presenting with a 10-day history of progressive headache and diplopia. Sagittal (a) and axial (b) MR angiography (1.5 T, time-of-flight) demonstrate a saccular aneurysm arising from the left posterior communicating artery (red arrows). Digital subtraction angiography (DSA) in sagittal projection (c) confirms the aneurysm, with 3D rotational reconstruction (d) characterizing its morphology and neck. Post-embolization control DSA (e) demonstrates complete aneurysm exclusion from the circulation (yellow arrow). All images are fully anonymized and reproduced with written patient consent.*

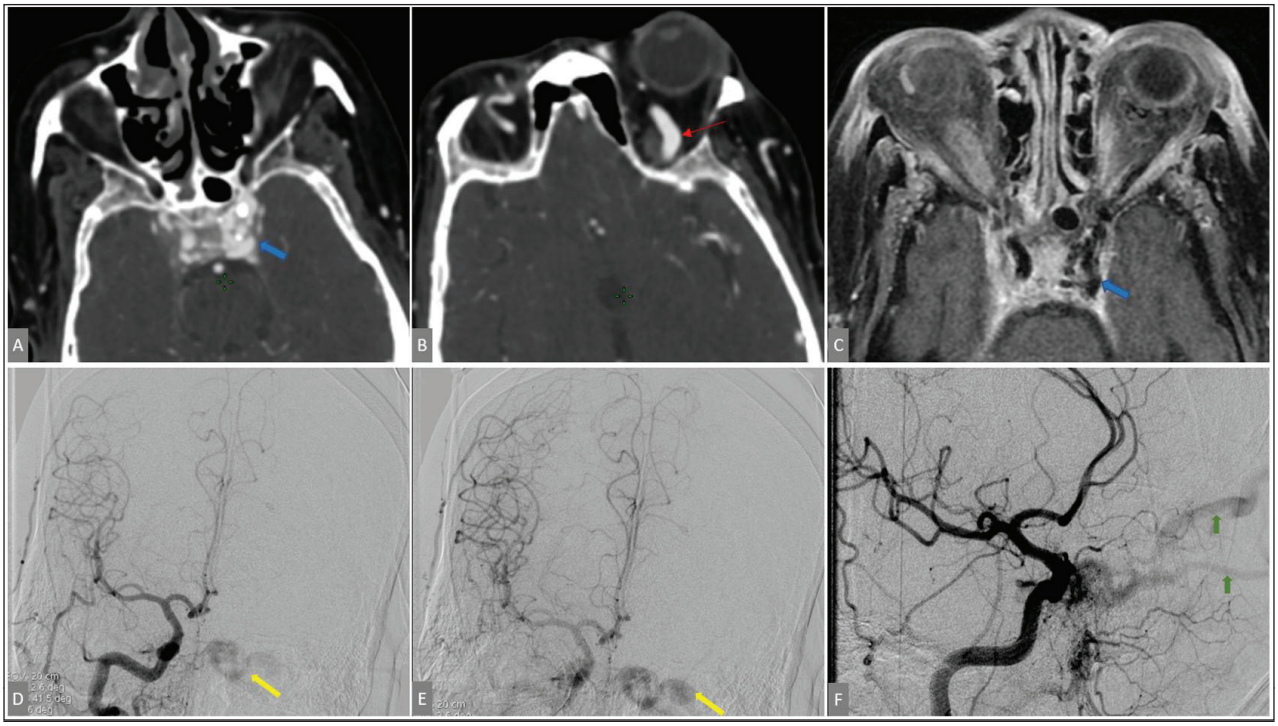

Figure 5. *A 46-year-old man with a history of hypertension and diabetes, presenting with a 2-day history of headache and left eyelid ptosis. Axial contrast-enhanced CT in the arterial phase (a, b) demonstrates early opacification of the left cavernous sinus (a) and dilatation of the left superior ophthalmic vein (b), suggestive of a carotid-cavernous fistula. Axial T2-weighted fat-saturated MRI (1.5 T) (c) shows serpiginous flow voids within the left cavernous sinus, reflecting arteriovenous shunting. DSA performed during opacification of the right internal carotid artery (d–f) confirms early filling of the left cavernous sinus (yellow arrow) with retrograde drainage through both superior ophthalmic veins (green arrows), consistent with a spontaneous dural carotid-cavernous fistula. All images are fully anonymized and reproduced with written patient consent.*

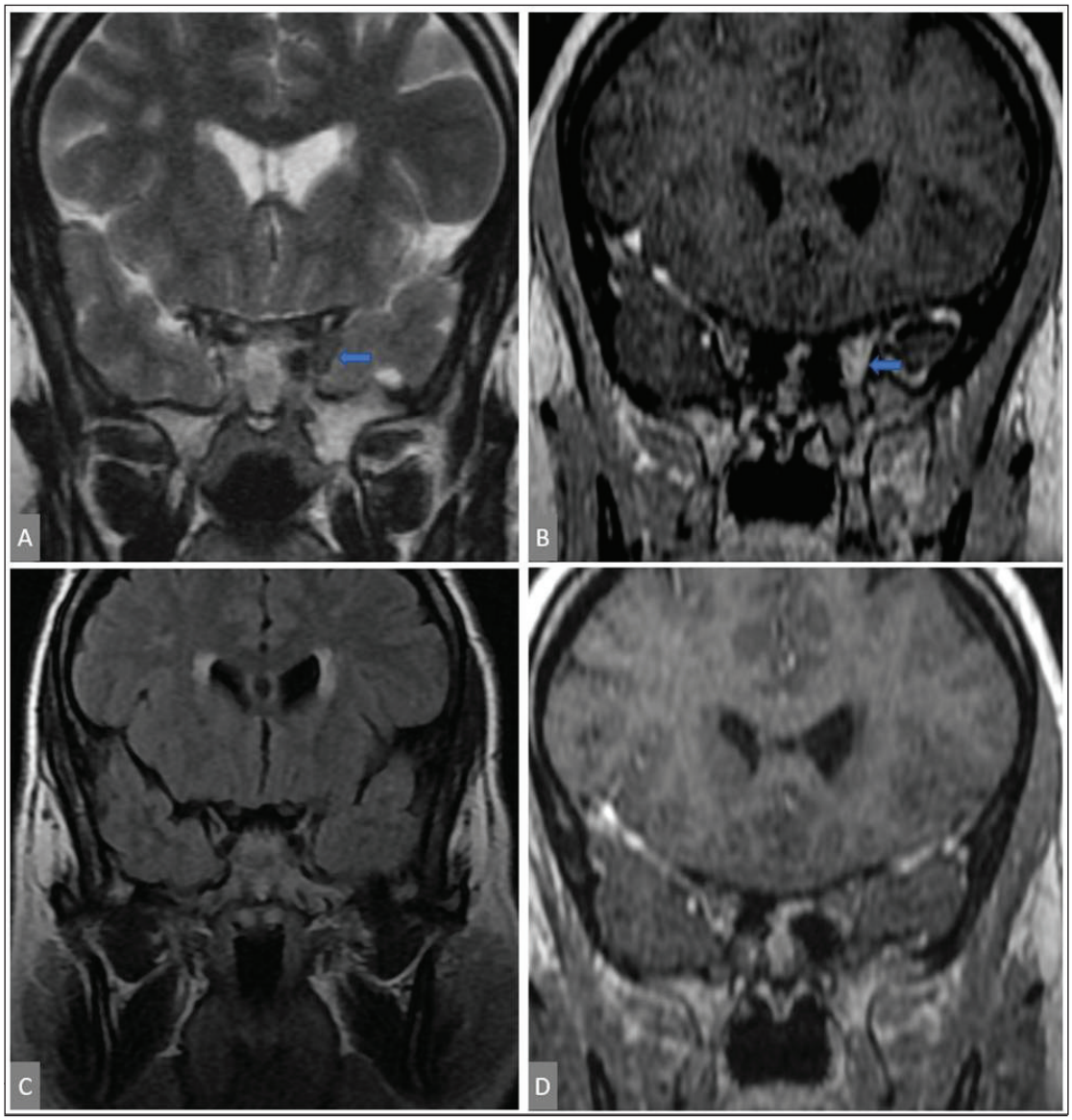

Figure 6. *A 32-year-old woman presenting with sudden-onset left orbital pain, diplopia, and ptosis of 1-day duration. Coronal T2-weighted (a) and post-contrast T1-weighted MRI (1.5 T) (b) demonstrate an infiltrative lesion involving the left orbital apex and cavernous sinus, with intermediate T2 signal and homogeneous enhancement, without bone destruction or discrete mass formation, consistent with an inflammatory process. Diagnosis of Tolosa–Hunt syndrome was established according to International Classification of Headache Disorders 3rd edition criteria, following systematic exclusion of neoplastic, infectious, and vascular mimics. Corticosteroid response and radiological resolution on follow-up MRI at 6 months (c, d) supported the diagnosis. All images are fully anonymized and reproduced with written patient consent.*

achieved complete recovery while three experienced partial recovery.

Aneurysms appeared as saccular dilatations on CT/MR angiography, confirmed by DSA. The posterior communicating artery aneurysm was treated by endovascular coiling with subsequent CN III recovery, while the ICA aneurysm was managed by surgical clipping with partial recovery (Figure 4).

CCFs demonstrated arteriovenous shunting, characterized by a dilated superior ophthalmic vein and early venous filling. Both were spontaneous, detected on CT/MRI, and confirmed by DSA. Both patients underwent endovascular embolization with good orbital recovery (Figure 5).

Vascular lesions were more frequently associated with acute onset and prominent orbital signs such as proptosis and chemosis.

3. Inflammatory etiologies (n = 2, 8%)

Tolosa–Hunt syndrome (n = 1) and orbital pseudotumor (n = 1) were diagnosed following systematic exclusion of neoplastic and infectious mimics.

Tolosa–Hunt syndrome presented on MRI as ill-defined cavernous sinus soft-tissue thickening with homogeneous enhancement, without a discrete mass or bone destruction. Diagnosis was established according to International Classification of Headache Disorders 3rd edition (ICHD-3) criteria, following a negative workup including complete blood count, inflammatory markers

(C-reactive protein and erythrocyte sedimentation rate), serum angiotensin-converting enzyme, antinuclear antibodies, antineutrophil cytoplasmic antibodies, thyroid function tests, and cerebrospinal fluid analysis, combined with multidisciplinary assessment by neurologists and ophthalmologists. Complete response to corticosteroids, confirmed on 6-month follow-up MRI, supported the diagnosis (Figure 6).

Orbital pseudotumor presented as T2-hypointense infiltrative orbital and cavernous sinus involvement with delayed enhancement. Infection and malignancy were excluded through clinical and radiological assessment. The patient responded well to corticosteroids and was maintained on follow-up.

In both cases, the absence of bone destruction, lack of a discrete mass, negative exclusion workup, and favorable corticosteroid response were collectively supportive of the inflammatory diagnosis.

Discussion

CSS represents a diagnostic challenge owing to the complex anatomical configuration of the cavernous sinus and the wide spectrum of underlying pathologies that may produce similar clinical presentations. In this context, imaging plays a crucial role in confirming cavernous sinus involvement and narrowing the differential diagnosis based on characteristic patterns.

This retrospective observational study highlights the significance of a systematic multimodal imaging approach in determining the underlying etiology of CSS, even when MRI was accessible to only 50% of the cohort. Neoplastic causes predominated (62%), consistent with the landmark Barcelona series by Fernández et al., in which tumors accounted for 63% of cases. In contrast, vascular lesions were less frequent, representing approximately 20% of cases [4]. Both cohorts highlight the significance of direct parasellar invasion or compressive effects from lesions, such as meningiomas, pituitary macroadenomas, and skull base tumors. Similarly, a large North American series by Keane identified neoplasms as the primary etiology, emphasizing that compressive or infiltrative processes continue to be the predominant mechanisms in Western populations [1].

Geographic and epidemiological differences were apparent when contrasting our findings with data from high-burden regions in South Asia. Bhatkar et al. reported neoplasms in only 28.8% of the cases, with inflammatory and infectious processes, particularly fungal sinusitis, representing a larger proportion [5]. Similarly, Rodge et al. identified Tolosa–Hunt syndrome and infectious etiologies as the primary causes [6]. These differences likely stem from variations in the prevalence of diabetes, environmental exposure to opportunistic pathogens, and access to healthcare, all influencing disease presentation and progression.

From an imaging perspective, distinguishing cavernous sinus lesions relies on pattern recognition combined with precise anatomical localization [7]. Neoplastic processes are usually identified by a distinct mass located in the parasellar or skull base region, frequently linked with mass effects and expansion into the cavernous sinus. Specific features further aided characterization: a dural tail and adjacent bone remodeling favored meningioma, while infiltrative soft-tissue extension across anatomical boundaries suggested lymphoma or nasopharyngeal carcinoma. Pituitary macroadenomas were identified by their sellar origin and lateral extension, often showing encasement of the intracavernous internal carotid artery without notable luminal narrowing, a crucial diagnostic feature [2,3].

In contrast, vascular lesions were defined by flow-related or luminal abnormalities, rather than true masses. Cavernous sinus thrombosis appeared as an intraluminal filling defect with absence of normal flow voids, frequently associated with dilation of the superior ophthalmic vein. In our cohort, all four cases of cavernous sinus thrombosis were of septic origin: two complicated orbital cellulitis and two sphenoidal sinusitis. All patients received anticoagulation combined with broad-spectrum antibiotic therapy, consistent with established management guidelines; one achieved complete recovery while three experienced only partial recovery. Carotid-cavernous fistulas exhibited arterialized venous drainage with early venous enhancement, while aneurysms were identified as focal vascular dilatations contiguous with arterial structures, best characterized by angiographic methods [2].

Inflammatory conditions present a significant diagnostic challenge due to the absence of a well-defined mass, instead appearing as ill-defined soft-tissue thickening with homogeneous enhancement. The absence of bone destruction or significant mass effect, along with the clinical context, was crucial in suggesting diagnoses such as Tolosa–Hunt syndrome or inflammatory pseudotumor. In both inflammatory cases in our cohort, the diagnosis was established only after systematic exclusion of neoplastic and infectious mimics through comprehensive laboratory workup and multidisciplinary assessment. Corticosteroid response and radiological resolution on follow-up imaging served as supportive findings, consistent with the diagnostic criteria for Tolosa–Hunt syndrome under the ICHD-3 classification [8].

These imaging patterns, consistent with prior radiological descriptions, emphasize the significance of a structured, anatomy-based approach to cavernous sinus assessment [2,3]. Moreover, the consistent initial use of CT in our study was effective for rapid triage, particularly in settings with limited MRI availability, enabling early detection of bone involvement and major vascular

complications [9]. However, CT has inherent limitations in assessing soft-tissue extent, perineural spread, and subtle inflammatory changes and should be considered complementary to MRI rather than a standalone diagnostic tool in this context.

In addition to diagnosis, imaging findings have direct therapeutic implications. Rapid identification of vascular etiologies, such as cavernous sinus thrombosis or carotid-cavernous fistula, is crucial for initiating prompt treatment, while recognizing neoplastic invasion guides biopsy and oncological management. Accurately differentiating inflammatory conditions helps prevent the inappropriate use of corticosteroids in infectious or malignant processes [10].

Limitations of this study include its retrospective, single-center design and relatively small sample size. Incomplete MRI utilization reflects real-world resource constraints and may have limited the detection of subtle lesions. Follow-up was incomplete in a subset of patients, with two lost to follow-up and one deceased, limiting outcome assessment. Additionally, referral bias may have favored more advanced presentations. However, the strengths of the study comprise the consecutive inclusion of all eligible patients over a defined four-year period, consistent multimodal imaging correlation, and the contribution of data from a North African population that remains underrepresented in the published literature.

Conclusion

CSS includes a diverse range of conditions with overlapping clinical features, where imaging plays a crucial role in diagnosis. Multimodal evaluation, particularly contrast-enhanced MRI combined with CT and vascular imaging, contributed to etiological characterization and management planning in this cohort.

Our findings highlight the predominance of neoplastic and vascular etiologies in this North African setting, with an etiologic distribution that differs from those reported in Western and South Asian series. A prompt and systematic cross-sectional evaluation is crucial to prevent diagnostic delays and to guide the appropriate management of potentially reversible or life-threatening conditions.

What is new?

CSS presents a wide diagnostic spectrum in which imaging plays a pivotal role. In this North African cohort, neoplastic and vascular etiologies predominated, differing from patterns reported in other regions. A structured multimodal imaging approach contributes to accurate diagnosis and guides timely management.

Acknowledgments

None.

List of Abbreviations

CN	cranial nerve
CSS	cavernous sinus syndrome
CT	computed tomography
DSA	digital subtraction angiography
FLAIR	fluid-attenuated inversion recovery
ICA	internal carotid artery
MRA	magnetic resonance angiography
MRI	magnetic resonance imaging
MRV	magnetic resonance venography
PComA	posterior communicating artery
UCNT	undifferentiated carcinoma of the nasopharyngeal type

Conflict of interest

The authors declare that there is no conflict of interest regarding the publication of this article.

Funding

None.

Informed Consent

Written informed consent was obtained from all 26 patients included in this study, covering participation in the study and publication of clinical data and accompanying images. For the pediatric patient (patient 1), consent was obtained from the parents. For the deceased patient (patient 22), consent was obtained from the next of kin. For patients lost to follow-up (patients 18 and 21), consent was obtained at their last available clinical visit.

Ethical Approval

This study was approved by the Comité d'Éthique Hospitalo-Universitaire de Fès, University Hospital Hassan II, Fez, Morocco (approval number: 02/2025), prior to data extraction, analysis, and manuscript preparation. Although the clinical records reviewed span the period from January 2021 to December 2024, all data were extracted retrospectively from existing medical records following ethics approval in 2025. No prospective data collection or patient contact was performed. The study was conducted in accordance with the ethical principles of the Declaration of Helsinki.

Author details

Wiame Bougrine[1,2], Brahim El Mahjoub[1,2], Hajar Ouazzani Chahdi[2], Ismail Chaouche[1], Amal Akammar[2], Nizar El Bouardi[1], Meriem Haloua[2], Badreeddine Alami[1], Mly Youssef Alaoui Lamrani[1], Mustapha Maaroufi[1] and Meryem Boubbou[2]

1. Department of Adult Radiology, University Hospital CHU Hassan II, Faculty of Medicine and Pharmacy, Sidi Mohamed Ben Abdellah University, Fez, Morocco
2. Department of Mother and Child Radiology, University Hospital CHU Hassan II, Faculty of Medicine and Pharmacy, Sidi Mohamed Ben Abdellah University, Fez, Morocco

References

1. Keane JR. Cavernous sinus syndrome: analysis of 151 cases. Arch Neurol. 1996;53(10):967–71. https://doi.org/10.1001/archneur.1996.00550100077015
2. Razek AA, Castillo M. Imaging lesions of the cavernous sinus. Am J Neuroradiol. 2009;30(3):444–52. https://doi.org/10.3174/ajnr.A1372
3. Mahalingam HV, Khurana A, Gupta K, Bhatt S, Bhatt ML, Khandelwal N, et al. Imaging spectrum of cavernous sinus lesions with histopathologic correlation. Radiographics. 2019;39(3):795–817. https://doi.org/10.1148/rg.2019180122

4. Fernández S, Godino O, Martínez-Yélamos S, Mesa E, Arruga J, Ramón JM, et al. Cavernous sinus syndrome: a series of 126 patients. Medicine (Baltimore). 2007;86(5):278–81. https://doi.org/10.1097/MD.0b013e31814b80c1
5. Bhatkar S, Goyal MK, Takkar A, Mukherjee KK, Prabhakar S, Lal V, et al. Cavernous sinus syndrome: a prospective study of 73 cases at a tertiary care center in Northern India. Clin Neurol Neurosurg. 2017;155:63–9. https://doi.org/10.1016/j.clineuro.2017.02.006
6. Rodge VN, Mukherjee A, Biswas S, Pandit A, Lahiri D, Roy MK, et al. Clinical and radiological profile of cavernous sinus syndrome: a study from eastern India. Egypt J Neurol Psychiatr Neurosurg. 2023;59:64. https://doi.org/10.1186/s41983-023-00667-x
7. Kapoor K, Singh B, Dewan LI. Anatomical variations of the cavernous sinus and its clinical implications. J Clin Diagn Res. 2014;8(12):AC01–04. https://doi.org/10.7860/JCDR/2014/10323.5270
8. Thomas TD, Trobe JD, Cornblath WT. Tolosa-Hunt syndrome: the spectrum of disease. Ophthalmology. 2000;107(2):337–43. https://doi.org/10.1016/S0161-6420(99)00067-3
9. Friedman DI, Jacobson DM. Diagnostic approach to painful ophthalmoplegia. Am J Ophthalmol. 2002;134(4):591–9. https://doi.org/10.1016/S0002-9394(02)01651-2
10. Miller NR. Primary and secondary causes of cavernous sinus syndrome. J Neuro-Ophthalmol. 2015;35(3):288–99. https://doi.org/10.1097/WNO.0000000000000271